Monthly Notices of the ROYAL ASTRONOMICAL SOCIETY

MNRAS **536,** 314–323 (2025) https://doi.org/10.1093/mnras/stae2748
Advance Access publication 2024 December 12

EDGE: dark matter core creation depends on the timing of star formation

Claudia Muni [1]★ Andrew Pontzen,[2] Justin I. Read [3] Oscar Agertz [4] Martin P. Rey [5,6] Ethan Taylor,[3] Stacy Y. Kim[7] and Emily I. Gray [3]

[1]*Department of Physics & Astronomy, University College London, Gower Street, London WC1E 6BT, UK*
[2]*Institute for Computational Cosmology, Department of Physics, Durham University, South Road, Durham DH1 3LE, UK*
[3]*Department of Physics, University of Surrey, Surrey, Guildford GU2 7XH, UK*
[4]*Lund Observatory, Division of Astrophysics, Department of Physics, Lund University, Box 43, SE-22100 Lund, Sweden*
[5]*Sub-department of Astrophysics, Department of Physics, University of Oxford, DWB, Keble Road, Oxford OX1 3RH, UK*
[6]*Department of Physics, University of Bath, Claverton Down, Bath BA2 7AY, UK*
[7]*Carnegie Theoretical Astrophysics Center, Carnegie Observatories, 813 Santa Barbara Street, Pasadena, CA 91106, USA*

Accepted 2024 December 10. Received 2024 November 26; in original form 2024 September 11

ABSTRACT

We study feedback-driven cold dark matter core creation in the EDGE suite of radiation-hydrodynamical dwarf galaxy simulations. Understanding this process is crucial when using observed dwarf galaxies to constrain the particle nature of dark matter. While previous studies have shown that the stellar mass to halo mass ratio ($M_\star/M_{200}$) determines the extent of core creation, we find that in low-mass dwarfs there is a crucial additional effect, namely the timing of star formation relative to reionization. Sustained post-reionization star formation decreases central dark matter density through potential fluctuations; conversely, pre-reionization star formation is too short-lived to have such an effect. In fact, large stellar masses accrued prior to reionization are a strong indicator of early collapse, and therefore indicative of an *increased* central dark matter density. We parametrize this differentiated effect by considering $M_{\star,\rm post}/M_{\star,\rm pre}$, where the numerator and denominator represent the stellar mass formed after and before $z \sim 6.5$, respectively. Our study covers the halo mass range 10^9 M$_\odot$ $< M_{200} < 10^{10}$ M$_\odot$ (stellar masses in the range 10^4 M$_\odot$ $< M_\star < 10^8$ M$_\odot$), spanning both ultra-faint and classical dwarfs. In this regime, $M_{\star,\rm post}/M_{\star,\rm pre}$ correlates almost perfectly with the central dark matter density at $z = 0$, even when including simulations with a substantially different variant of feedback and cooling. We provide fitting formulae to describe the new-found dependence.

Key words: galaxies: dwarf – galaxies: haloes – dark matter.

1 INTRODUCTION

Dwarf galaxies can offer insights into the particle nature of dark matter. Their abundance is indicative of the small-scale cosmological power spectrum and can place constraints on scenarios such as warm dark matter (e.g. Schneider et al. 2012; Newton et al. 2021). Their central dark matter densities, which can be estimated from kinematic analyses (e.g. Binney & Mamon 1982; Adams et al. 2014; Zoutendijk et al. 2021), place limits on the strength of self-interacting dark matter (e.g. Yoshida et al. 2000; Rocha et al. 2013; see also Tulin & Yu 2018 for a review) or on the mass of fuzzy dark matter candidates (e.g. Hu, Barkana & Gruzinov 2000; Schive et al. 2014; Mina, Mota & Winther 2022). However, the effect of feedback from stellar populations is also particularly strong in these low-mass galaxies due to their shallow potential wells. This baryonic imprint is hard to calculate and substantially complicates the interpretation of observations (e.g. Dekel & Silk 1986; Efstathiou 1992, 2000; Benson et al. 2002; Pontzen & Governato 2014; Bullock & Boylan-Kolchin 2017).

Simulations have established that baryonic physics plays an important role in shaping the density profiles of low-mass dark matter haloes (e.g. Read & Gilmore 2005; Mashchenko, Wadsley & Couchman 2008; Governato et al. 2010; Pontzen & Governato 2012; Oñorbe et al. 2015; Benítez-Llambay et al. 2019). The 'dark matter heating' model (see Pontzen & Governato 2014 for a review) suggests that potential fluctuations caused by the supernova (SN) explosions and other feedback-driven outflows can inject energy into the dark matter particles, causing them to migrate outwards. This process therefore turns the dense dark matter 'cusps' expected from pure cold dark matter (CDM) simulations (e.g. Navarro, Eke & Frenk 1996; Read & Gilmore 2005; Teyssier et al. 2013; Di Cintio et al. 2014; Read, Agertz & Collins 2016) into 'cores' of near-constant density. While a single blow-out cannot transform cusps into cores (Gnedin & Zhao 2002), repeated fluctuations from cycles of gas cooling and feedback can disrupt the dark matter particles' orbits, causing the halo to expand and eventually flattening the inner regions of the density profiles. The inner density can also be lowered through a combination of stellar feedback and dynamical friction heating from subhaloes, gas clouds, and/or star clusters (Orkney et al. 2021; see also El-Zant, Shlosman & Hoffman 2001; Nipoti & Binney 2014).

The stellar-to-halo mass ratio ($M_\star/M_{200}$) is a primary determinant of the extent of baryonic core creation processes at $z = 0$ (Peñarrubia et al. 2012; Di Cintio et al. 2013, 2014; Tollet et al. 2016; Bouché et al. 2022; De Leo et al. 2024). The ratio $M_\star/M_{200}$ itself varies

★ E-mail: claudia.muni.21@ucl.ac.uk

systematically with mass M_{200} (e.g. Behroozi, Conroy & Wechsler 2010; Moster, Naab & White 2013; Garrison-Kimmel et al. 2017; Read et al. 2017; Nadler et al. 2020; Munshi et al. 2021; Danieli et al. 2023). In smaller haloes, with low $M_\star/M_{200}$, stellar feedback is too weak to significantly alter the trajectories of the dark matter particles, resulting in cuspy inner density profiles. As the stellar mass increases, feedback becomes sufficiently strong to turn dark matter cusps into cores (Peñarrubia et al. 2012; Read, Walker & Steger 2019). As the $M_\star/M_{200}$ ratio increases further, the pressurization of the interstellar medium becomes high enough that SNe cannot generate coherent potential fluctuations across the galaxy as a whole, making dark matter heating inefficient once more. This picture has been shown to provide qualitative agreement with observations of real galaxies for $-3 \lesssim \log(M_\star/M_{200}) \lesssim -1.75$, although the uncertainties in the data remain high (Read et al. 2019; Bouché et al. 2022; Collins & Read 2022; Cooke et al. 2022).

However, there is no theoretical guarantee that $M_\star/M_{200}$ is the *sole* determinant of core size and shape. From simulations, Chan et al. (2015) noted that star formation that is contemporaneous with rapid halo collapse is inefficient at forming cores in simulations. Observationally, Oman et al. (2015) highlight significant diversity in dwarf irregular galaxy rotation curves at fixed stellar mass. While this may in part reflect observational biases from non-circular motions or holes driven by stellar feedback in the H I gas distributions (Read et al. 2016; Marasco et al. 2018; Oman et al. 2018; Roper et al. 2023), diversity in the observed population underscores the need for theoretical analyses that explore factors other than total stellar mass. This need is the focus of our investigation.

In this work, we analyse dark matter density profiles from the Engineering Dwarfs at Galaxy formation's Edge (EDGE) suite of state-of-the-art radiation-hydrodynamical simulations of dwarf galaxies (Agertz et al. 2020). We include simulations from both the EDGE1 and EDGE2 suites, the latter of which has updated physics that we will describe shortly. To study the impact of baryonic feedback, we focus primarily on the central halo density measured at $r = 150$ pc, a radius at which observational density estimates may be made both in dwarf spheroidal and irregular galaxies (Read et al. 2019). The cusp-core transformation process acts to lower this density. We analyse the main factors that drive the core creation, showing that the *timing* of star formation has an important bearing, one which is not captured by $M_\star/M_{200}$. This is in agreement with the basic physics of dark matter heating through potential fluctuations, as discussed above, but has hitherto received limited attention.

This paper is organized as follows. Section 2 gives an overview of the EDGE2 simulations' physics and how it differs from the previous simulation suite (EDGE1), and an outline of the analysis pipeline. In Section 3, we present our key results and motivate the need for a new quantity that can represent the effect of feedback on EDGE haloes better than the widely used stellar-to-halo mass ratio ($M_\star/M_{200}$). In Section 4, we present our conclusions and discuss future theoretical and observational prospects.

2 SIMULATIONS

EDGE2 is a state-of-the-art suite of radiation-hydrodynamical dwarf galaxy simulations. The suite covers the mass range 10^9 M$_\odot$ < M_{200} < 10^{10} M$_\odot$ (corresponding to 10^4 M$_\odot$ < $M_\star$ < 10^8 M$_\odot$ in stellar masses). The numerical resolution is the same as in the previous EDGE1 runs (dark matter particle mass $m_{\rm DM} = 940$ M$_\odot$, and maximum spatial resolution in hydrodynamics and gravity of $\Delta x \approx 3$ pc), but the original galaxy formation model (described in detail in Agertz et al. 2020; Rey et al. 2020) has been significantly updated.

Some of the most notable changes introduced in EDGE2 are

(i) a new implementation of non-equilibrium cooling, which follows Rosdahl et al. (2013), modified from the equilibrium cooling from Courty & Alimi (2004) used in EDGE1;
(ii) the inclusion of photoionization feedback using radiative transfer following the set-up described in Agertz et al. (2020) across all the simulated haloes; and
(iii) an update of the ultraviolet (UV) background from a modified Haardt & Madau (1996) model (see Rey et al. 2020 for a discussion) to the Faucher-Giguère (2020) photoionization and photoheating rates.

A more detailed description of all the changes introduced in the new EDGE2 simulations will be provided in an upcoming paper (Rey et al., in preparation).

In this paper, we look at eight isolated dark matter haloes taken from the EDGE2 simulations, each hosting a dwarf galaxy. Six of the eight haloes are re-runs of EDGE1 objects,[1] and can therefore be used as direct comparisons to study the effects of different feedback recipes. Halo261 and Halo339 are new to the EDGE2 simulation suite.

The dwarf galaxies are all evolved in isolated cosmological environments (i.e. they are not satellites). The high resolution allows us to model SN explosions as discrete events and to track their effects on the galaxies explicitly, removing the uncertainties of modelling these processes as sub-grid physics. Our galaxies are evolved to $z = 0$ from cosmological zoomed initial conditions constructed with the GENETIC software (Stopyra et al. 2021). All our simulations use the parameters $\Omega_m = 0.3086$, $\Omega_\Lambda = 0.6914$, $h = 0.6777$, $\sigma_8 = 0.8288$, and $n_s = 0.9611$, which are compatible with Planck Collaboration XVI (2014). We follow the evolution of dark matter, stars, gas, and radiation using the adaptive mesh refinement hydrodynamics code RAMSES-RT (Teyssier 2002; Rosdahl et al. 2013). The star formation criteria in EDGE2 remain unchanged from EDGE1.

We process each EDGE2 simulation with the ADAPTAHOP halo and subhalo finder (Aubert, Pichon & Colombi 2004; Tweed et al. 2009). EDGE1 simulations are processed with the HOP halo finder (with parameters as described in Eisenstein & Hut 1998). Because we study the deep interior of the major progenitor of a single galaxy in each simulation, we do not expect the difference in halo finders to have any bearing on our results. We match haloes and subhaloes between simulation snapshots to build merger trees using the PYNBODY (Pontzen et al. 2013) and TANGOS (Pontzen & Tremmel 2018) libraries, in an identical way between the two EDGE versions. Halo centres are identified using the shrinking-sphere algorithm (Power et al. 2003), and densities estimated by binning particles. We use 100 log-spaced bins of width ranging approximately from 2×10^{-3} to 2.9 kpc, and smooth them over a moving window of 20 bins. Densities are shown exterior to 30 pc, which is sufficient to ensure that numerical softening effects are strongly subdominant (Muni et al. 2023).

Where we show errors on densities, these are found by calculating the Poisson noise in each bin and then using standard Gaussian error propagation to estimate an error on the moving-average quantities; however, these statistical errors are typically small since our simulations are well resolved. While in the future we will use improved

[1] These are Halo1445, 1459, 600, 605, 624, and 383. The complete suite was first introduced in Orkney et al. (2021), Rey et al. (2022), and Gray et al. (2024).

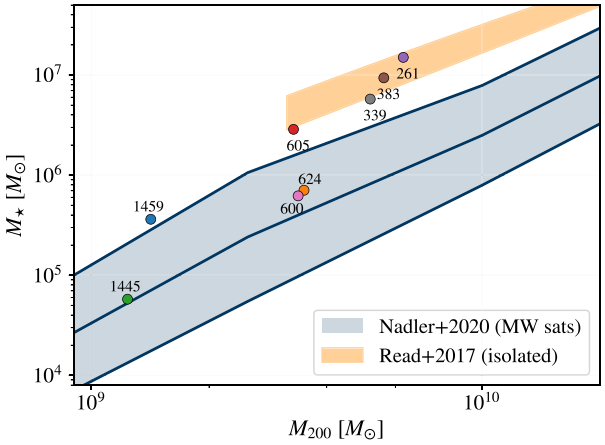

Figure 1. SMHM relation of the EDGE2 haloes. Abundance matching relations from real dwarfs are shown in blue and orange. The blue shading (spanning the entire halo mass range) shows the 16–84 per cent confidence interval for MW satellites from Nadler et al. (2020). The orange shading (spanning only the high mass region) is obtained from isolated dwarfs in Read et al. (2017). The EDGE2 results agree well with the MW satellites' relation for small values of M_{200} where the star formation rate is predominantly regulated by reionization quenching. As the halo mass grows, environmental effect becomes significant and the EDGE2 results show better agreement with the relation from isolated dwarfs.

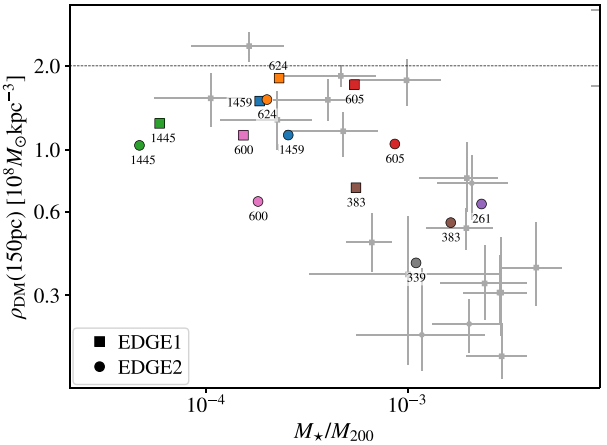

Figure 2. Dark matter density at $r = 150$ pc as a function of the stellar-to-halo mass ratio in the EDGE2 and EDGE1 haloes, shown as circles and squares, respectively. The EDGE2 simulations have an updated physics model compared to EDGE1, as discussed in Section 2. The Poisson errors on the dark matter densities are small (of the order of a few per cent) and therefore not visible in the figure. The light grey points represent dwarf galaxies data from Read et al. (2019). The horizontal dashed line shows the expected inner density for a Lambda-CDM (ΛCDM) cosmology at the mass scale of the EDGE haloes. The EDGE results show qualitative agreement with the data; however, there is considerable scatter both in the simulations and the observations (although the latter has large statistical uncertainties). This suggests that the $M_\star/M_{200}$ ratio alone is not sufficient to predict central dark matter density profiles.

dynamics-based density estimators (Muni et al. 2023), for this initial work the statistical errors are strongly subdominant to the trends of interest.

3 RESULTS

3.1 Stellar-to-halo mass relation

Fig. 1 shows the stellar mass–halo mass (SMHM) relation measured for the EDGE2 haloes. We take M_{200} to be the mass enclosed by r_{200}, the radius within which the mean density is 200 times higher than the critical density. We can approximately divide our EDGE2 haloes into three categories: 1445 and 1459 with lower halo masses ($\sim 10^9$ M$_\odot$); 600, 605, and 624 with intermediate halo masses ($\sim 3 \times 10^9$ M$_\odot$); and 339, 383, and 261 with larger M_{200} ($\sim 4 \times 10^9$ M$_\odot$). We notice that even when the haloes have similar M_{200}, their $M_\star$ can vary significantly, showing a dependence of stellar mass on the formation history (see Rey et al. 2019).

The bands in Fig. 1 allow us to compare our results with two empirical relations obtained from abundance matching in observed dwarf galaxies: Read et al. (2017), which refers to isolated dwarf galaxies similar to our simulated objects, but only covers the high-mass range of our sample; and Nadler et al. (2020), which spans the correct mass range for our haloes, but is obtained from Milky Way (MW) satellites' data.

In the low- and intermediate-mass regimes, the agreement between the EDGE2 data and the MW satellites' relation is good; our stellar masses are at the upper end of the observationally inferred range, but this can likely be explained by our galaxies being isolated rather than satellites (although see Christensen et al. 2024). The duration of star formation of ultra-faint dwarfs over time is mostly controlled by reionization quenching, but in MW satellites one would expect a secondary environmental effect from tides, stripping, and other disruption (e.g. Shipp et al. 2018; Mutlu-Pakdil et al. 2019; Weerasooriya et al. 2023). In the larger mass regime, these environmental effects may be a dominant factor in the MW satellite population since reionization does not quench them (e.g. Fattahi et al. 2018; Pace, Erkal & Li 2022). In these cases, our simulations form too many stars to be compatible with MW satellite observations, but are in excellent agreement with the relation from isolated galaxies. See Rey et al. (in preparation) for a more detailed discussion on the SMHM relation in EDGE2, and Kim et al. (2024) for a semi-analytical code calibrated to predict EDGE stellar masses across a much larger statistical sample of dwarf galaxies.

Our simulations are not specifically tuned to reproduce the SMHM relation, and as such the comparison above gives some confidence. None the less, it should be viewed with caution. Nadler et al. (2020) advise that their model of the MW satellite SMHM is a useful empirical relation, but is not intended to capture the complexities of star formation in ultra-faint dwarfs, where there is a very strong sensitivity to accretion history (Rey et al. 2019; Kim et al. 2024). The behaviour of the Read et al. (2017) field relation for $M_\star \lesssim 4 \times 10^6$ M$_\odot$ is also unclear since a direct extrapolation to lower halo masses is not necessarily justified. Also, there is evidence that this relation is based on H I-rich dwarfs, which are outliers in stellar mass for their halo mass (Kim et al. 2024). In this context, we conclude that the EDGE2 results approximately span the correct stellar mass range given their halo masses, but there are still considerable uncertainties in how galaxies truly occupy the SMHM plane; future facilities such as the Vera Rubin Observatory will have a major impact on tightening these uncertainties (Simon 2019).

3.2 Core creation as a function of $M_\star/M_{200}$

Fig. 2 shows the dark matter density at $r = 150$ pc as a function of the stellar-to-halo mass ratio for our EDGE haloes. The observational significance of this radius was discussed in Section 1; from now

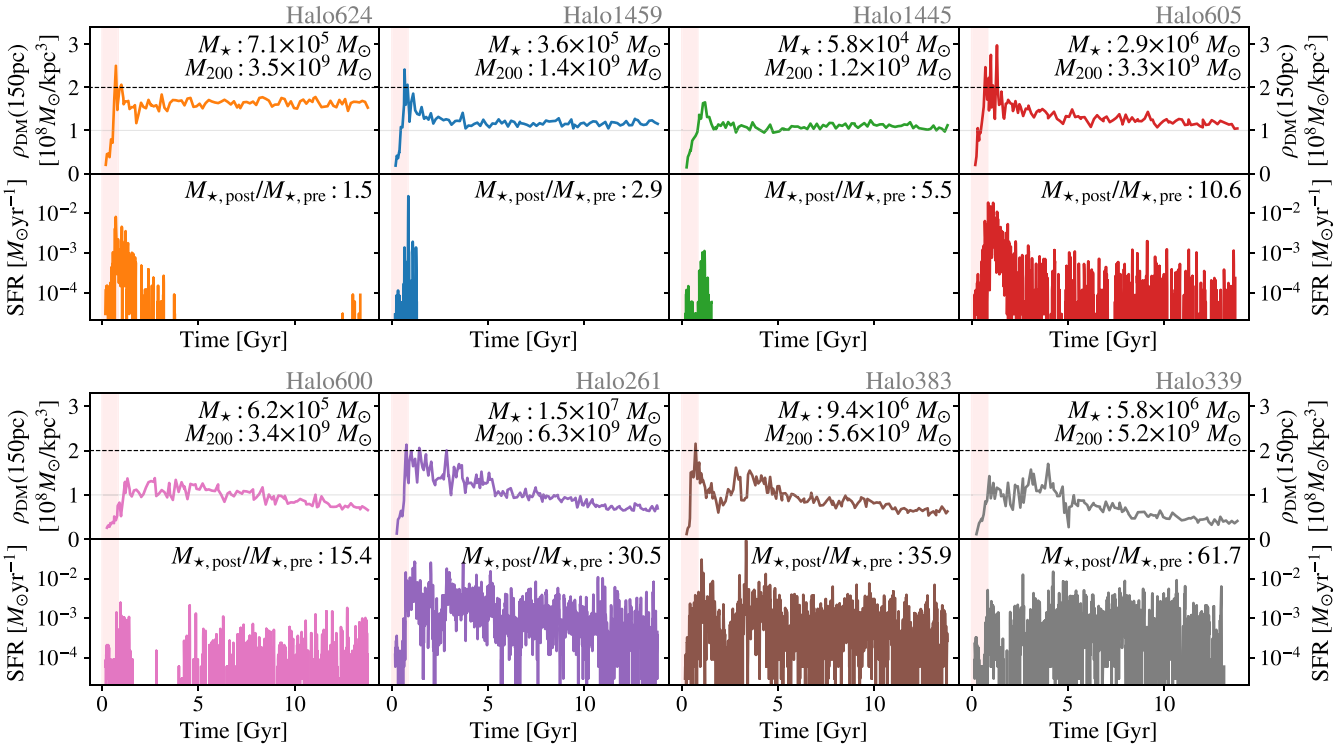

Figure 3. Evolution of the dark matter densities at 150 pc for the eight EDGE2 haloes (top rows) alongside their galaxies' SFHs (bottom rows) as a function of cosmic time since the big bang. The vertical pink shaded region shows the time prior to reionization ($z \lesssim 6.5$) and the horizontal dashed line at $\rho_{\rm DM} = 2 \times 10^8$ M$_\odot$ kpc^{-3} shows the expected density for a ΛCDM cosmology (same as in Fig. 2). The haloes are ordered according to their $M_{\star,{\rm post}}/M_{\star,{\rm pre}}$ ratio (the stellar mass post-reionization divided by the stellar mass prior to reionization). The first three haloes from the top retain cuspy profiles, while the rest of the haloes form cores of various sizes. Haloes that show star formation continuing until today display lower central dark matter densities; conversely, haloes that have early star formation reach higher concentrations before reionization, and therefore have higher inner densities at the present day.

on, we will refer for brevity to $\rho_{\rm DM}$ implying that it has been evaluated at this radius, unless otherwise specified. A higher value of the density $\rho_{\rm DM}$ corresponds to 'cuspier' haloes. The grey points show the values measured for real dwarf galaxies (both isolated and satellites) obtained from Read et al. (2019) (and references therein). Our simulation suite covers halo masses up to $\sim 10^{10}$ M$_\odot$, allowing us to probe only the low-mass end of this relation. The simulation densities and associated statistical uncertainties were calculated as described in Section 2, and the resulting Poisson errors are too small to display (ranging between 1.8×10^6 and 3.5×10^6 M$_\odot$ kpc^{-3}, i.e. of the order of a few per cent).

The results of the EDGE2 simulations (circles) show broad agreement with the data, with an average decrease in the central densities as the value of $M_\star/M_{200}$ increases, consistent also with the theoretical picture discussed in Section 1. However, there is significant scatter in the simulation results. The Pearson's coefficient for the combined EDGE1 and EDGE2 suites of simulations was found to be $r = -0.54$. Comparing pairs of haloes in EDGE2 such as Halo339 and Halo605, or Halo600 and Halo624, we obtain similar values of the $M_\star/M_{200}$ ratio, but diverse central dark matter densities, with variations up to a factor of 2.7. Conversely, Halo600, Halo383, and Halo261 all have similar values of $\rho_{\rm DM}$, but their stellar-to-halo mass ratio is extremely varied. The observational data are also compatible with these variations in $\rho_{\rm DM}$ at fixed $M_\star/M_{200}$, although the small sample size and large statistical uncertainties make it difficult to assess the population scatter quantitatively.

While the correlation of $\rho_{\rm DM}$ with $M_\star/M_{200}$ is clear in the EDGE2 simulations ($r = -0.58$) and the combined EDGE1+2 sample, if one removes the EDGE2 simulations (circles) and considers EDGE1 (squares) alone, there is no identifiable trend ($r = -0.13$). For example, Halo383 and Halo600 in EDGE1 both have high values of $M_\star/M_{200}$ but the former is cored and the latter is cuspy. Furthermore, Halo600 and Halo605 are cored in EDGE2 but retain high central densities in EDGE1, underscoring the impact of changing the feedback implementation (Section 2).

From the above, it appears that the $M_\star/M_{200}$ ratio alone is not a reliable indicator of the presence of cores in the EDGE haloes. The ratio does not capture essential information about the history of the galaxies, which affects the dark matter density at present day. We will next show that these results, including the differences between feedback recipes, can be explained once the timing of star formation is taken into account.

3.3 The importance of star formation timing

Fig. 3 shows the evolution over time of the dark matter density $\rho_{\rm DM}$ at our chosen radius ($r = 150$ pc) for the eight EDGE2 haloes (top rows) alongside the galaxies' star formation histories (SFHs; bottom rows), as a function of cosmic time since the big bang. The small fluctuations in $\rho_{\rm DM}$ arise from statistical noise due to the limited number of particles.

Halo1459, Halo624, and Halo1445 (first three in the top row) are the only haloes whose $\rho_{\rm DM}$ remains constant as time progresses, meaning that they retain steep cusps throughout their history. The inner gradients of the remaining haloes flatten over time forming

cores of various sizes.[2] The decrease in the central density of the cored haloes is gradual, underscoring that stellar feedback causes the dark matter halo to slowly expand over time through several smaller outflow episodes, rather than a single explosive incident.[3]

Among the cored haloes, we notice a correlation between their central densities and their virial masses (which is given in each panel), with more massive haloes showing progressively lower $\rho_{\rm DM}$ on average. The decrease in $\rho_{\rm DM}$ with M_{200} is consistent with the average decline in densities as a function of $M_\star/M_{200}$ in Fig. 2, since M_{200} and M_* are connected by the SMHM relation. However, as noted above for the stellar-to-halo mass ratio, there is considerable scatter around this trend. Taking, for example, the comparison between Halo600 and Halo624, both have almost identical M_{200} and $M_\star$ values but their final dark matter density is very different. The reason for this becomes clear when we compare the SFHs (bottom rows of Fig. 3). While Halo624 forms almost all its stars at high redshift, many of them before reionization, Halo600 builds up its stellar population predominantly at late times. As such, it proceeds through many more cycles of gas collapse, star formation, and gas expulsion; this cyclical engine is necessary to gradually reduce the dark matter density over time (Pontzen & Governato 2014). Moreover, because Halo624 collapses quickly at high redshift, its central cusp is more concentrated at early times, reaching a peak value of $\rho_{\rm DM} = 2.5 \times 10^8$ M$_\odot$ kpc^{-3} compared with Halo600's $\rho_{\rm DM} = 1.4 \times 10^8$ M$_\odot$ kpc^{-3}.

The link between earlier star formation and higher dark matter densities is further reinforced by comparing Halo600 with Halo605. Both objects have similar virial masses and extended star formation after reionization, yet the final density of Halo605 is $\rho_{\rm DM} = 1.0 \times 10^8$ M$_\odot$ kpc^{-3}, compared with the lower $\rho_{\rm DM} = 6.6 \times 10^7$ M$_\odot$ kpc^{-3} of Halo600. This is despite Halo605 forming *more* stars (2.9×10^6 M$_\odot$) than Halo600 (0.6×10^6 M$_\odot$); the central density trend is inverted with respect to expectations from $M_\star/M_{200}$. The inverted trend arises because Halo605 collapsed earlier, forming with a higher dark matter density than Halo600 at early times ($t \sim 2$ Gyr); consequently, the $z = 0$ dark matter density of the former remains high compared with the latter. This difference is correlated with early star formation, but not causally affected by it; we find that it is also present in the dark matter-only simulations, where the densities at $t \simeq 2$ Gyr are 1.4×10^8 M$_\odot$ kpc^{-3} for Halo600 and 2.6×10^8 M$_\odot$ kpc^{-3} for Halo605.

In summary, there are two separate mechanisms that link dark matter density and SFH. The difference between Halo600 and Halo624 can be causally explained by the amount of sustained, *late*-time star formation. A greater amount of sustained star formation leads directly to lower central densities, through the gravitational dynamics discussed in Section 1. Meanwhile, the difference between Halo600 and Halo605 can be explained by the high central concentration due to early collapse of the latter. *Early* star formation is correlated with higher central densities, since it is an indicator of early collapse and the feedback does not have time to significantly flatten the density profile.

[2]Note that the value of the density at 150 pc alone does not strictly indicate the presence of a cusp or core at $z = 0$. For a clearer understanding of why we refer to Halo1445, 1459, and 624 as cuspy and to the rest of the haloes in EDGE2 as cored, see the density profiles in Fig. 6.

[3]We do not observe any cores forming and then reverting back into cusps at later times; in the haloes where the gradient does not gradually flatten over time, the density remains constant over their entire history. This may be due to the limited sample size (see Section 4).

This perspective also explains the densities in the remaining EDGE2 haloes. The cuspy haloes (first three in the top row of Fig. 3) have already formed almost all of their stars by $z \sim 6$, while cored haloes see extended star formation until today, reducing their central dark matter density steadily over the Hubble time. Among the cored haloes, we see a correlation between the dark matter density and amount of stars formed at recent times: lower densities at $z = 0$ are linked to particularly active star formation post-reionization.

While there are a variety of ways in which one could divide star formation into 'early' and 'late' regimes, reionization provides a natural transition time. As mentioned in Section 1, reionization completely quenches low-mass dwarf galaxies. The smallest ultra-faint dwarf galaxies form all their stars at high redshift, before losing their gas. The most massive dwarfs, by contrast, have a sufficient potential depth and reservoir of dense gas by the time of reionization that they self-shield against the external ionizing radiation. In such cases, internal self-regulation is the primary factor limiting star formation rate, and reionization has only a secondary impact. In intermediate-mass cases, the timing of star formation is strongly dependent on the accretion history relative to reionization, and in some cases the galaxy may temporarily quench before later achieving a sufficient mass to restart star formation (Rey et al. 2019, 2020).

The pivotal role of reionization in these cases underscores why it forms a natural division between the two competing effects on the dark matter density. For the rest of our investigation, we will use

$$M_{\star,\rm post} = \int_{t=t_{\rm reion}}^{t_{\rm today}} \mathrm{SFR}\, \mathrm{d}t \tag{1}$$

(i.e. the amount of star formation that occurred in the galaxy's progenitors after reionization) as a proxy for the late-time star formation capable of flattening dark matter cusps. Conversely, we will use the quantity

$$M_{\star,\rm pre} = \int_{t=0}^{t_{\rm reion}} \mathrm{SFR}\, \mathrm{d}t \tag{2}$$

(i.e. the amount of star formation that occurred within the galaxy's progenitors prior to reionization) as a proxy for the early collapse, which encourages higher densities of dark matter. While reionization is a gradual process, we adopt $z \simeq 6.5$ ($t \simeq 0.84$ Gyr) when dividing the stellar populations. In Fig. 3, as well as in the calculation of $M_{\star,\rm post}$ and $M_{\star,\rm pre}$, we use the total mass formed at birth in the relevant stellar populations, rather than their remaining mass at $z = 0$, and we include stars formed in all progenitors of the galaxy (rather than just the major progenitor).

In Section 4, we will discuss these choices further, but our results below show that they successfully summarize a complex story in two simple competing effects. Specifically, we now explore the use of the $M_{\star,\rm post}/M_{\star,\rm pre}$ ratio as an indicator for the expected central density of CDM haloes.

3.4 The $M_{\star,\rm post}/M_{\star,\rm pre}$ ratio

In Fig. 4, we show the dark matter density profiles of the EDGE2 haloes. The y-axis has been multiplied by r^2 to emphasize the shape of the inner regions, and the profiles have been colour-coded based on the values of the galaxies' $M_{\star,\rm post}/M_{\star,\rm pre}$ ratio. Lighter colours indicate higher $M_{\star,\rm post}/M_{\star,\rm pre}$, i.e. star formation occurring at more recent times. The $M_{\star,\rm post}/M_{\star,\rm pre}$ ratio accurately correlates with the extent of core formation in the haloes: the higher the value, the lower the central density relative to the unmodified Navarro–Frenk–White (NFW) profile (black dashed line).

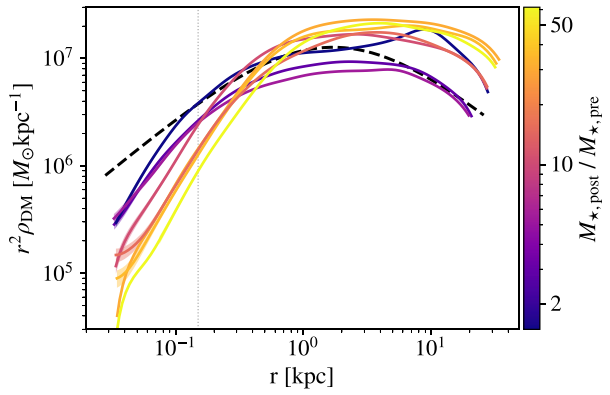

Figure 4. Dark matter density profiles of the EDGE2 haloes at $z = 0$, colour-coded by the value of their $M_{\star,\rm post}/M_{\star,\rm pre}$ ratio (the post-reionization stellar mass as a fraction of the stellar mass prior to reionization). The y-axis has been multiplied by r^2 to emphasize the inner regions. The NFW profile (dashed black line) for a dark matter halo of mass 2×10^8 M$_\odot$ and concentration $c = 15$ at $z = 0$ is shown for comparison. The vertical dotted line marks $r = 150$ pc. The shapes of the dark matter density profiles clearly depend on the galaxies' values of the $M_{\star,\rm post}/M_{\star,\rm pre}$ ratio, especially in the inner regions.

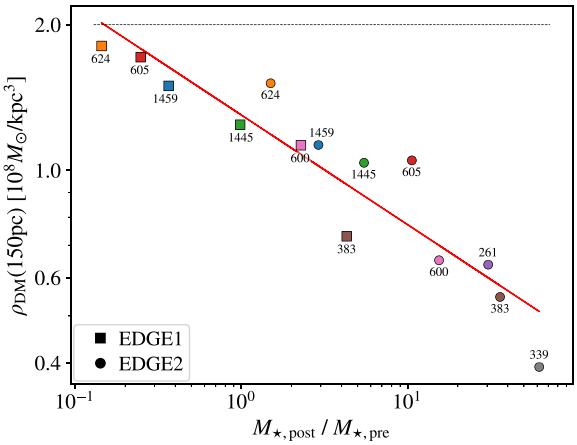

Figure 5. Dark matter density at 150 pc as a function of the $M_{\star,\rm post}/M_{\star,\rm pre}$ ratio. The circles show the EDGE2 haloes, while the squares are results from the EDGE1 simulations. A linear fit to the combined relation, given by equation (3), is shown in red. The horizontal dashed line shows the expected inner density from ΛCDM cosmology at the mass scale of the EDGE haloes. We notice a tight correspondence between the central dark matter density at $z = 0$ and $M_{\star,\rm post}/M_{\star,\rm pre}$, which was not captured by the $M_\star/M_{200}$ ratio.

Fig. 5 shows more quantitatively how $M_{\star,\rm post}/M_{\star,\rm pre}$ is predictive of the central density evaluated at a fixed 150 pc radius.

The correlation of this dark matter inner density is much stronger with $M_{\star,\rm post}/M_{\star,\rm pre}$ than with the stellar-to-halo mass ratio (Fig. 2), especially for the EDGE1 haloes (squares). If we fit these points with the relation

$$\log_{10}\rho_{\rm DM}(150\ {\rm pc}) = m\log_{10}\left(\frac{M_{\star,\rm post}}{M_{\star,\rm pre}}\right) + c, \quad (3)$$

the values of the coefficients for the combined sample are $m = -0.23 \pm 0.03$ and $c = 8.13 \pm 0.03$. This fit is shown as a red line in Fig. 5.

As examples of why the correlation has improved, consider the case of EDGE2 Halo600 contrasted with Halo383 and Halo261; as discussed in Section 3.2, Halo600 has a very different $M_\star/M_{200}$, but a similar value of $\rho_{\rm DM}$(150 pc). Fig. 5 highlights that Halo600 has an $M_{\star,\rm post}/M_{\star,\rm pre}$ ratio in approximate agreement with Halo383 and Halo261, making sense of the low central density. Similarly, Halo339 and Halo605 have comparable $M_\star/M_{200}$, but Halo605 underwent most of its star formation pre-reionization, resulting in a lower value of $M_{\star,\rm post}/M_{\star,\rm pre}$ and higher central dark matter density. In other words, what appeared as random scatter in Fig. 2 now appears as part of a tight trend in Fig. 5. We conclude that the scatter in the relationship between $M_\star/M_{200}$ and $\rho_{\rm DM}$ can be accounted for by the timing effects identified in Section 3.3.

Since the duration of star formation in dwarf galaxies is heavily controlled by reionization, our results are sensitive to the choice of separation time between pre- and post-reionization stars, especially for the haloes where $M_{\star,\rm post}$ is small. The dividing time we adopt ($t = 0.84$ Gyr) maximizes the Pearson's coefficient ($r = -0.93$) of the $\rho_{\rm DM}$–$M_{\star,\rm post}/M_{\star,\rm pre}$ relation for the combined suites of EDGE1 and EDGE2 simulations. This coefficient has a significantly increased magnitude compared with the correlation coefficient between $\rho_{\rm DM}$ and M_*/M_{200} ($r = -0.58$, see Section 3.2), indicating that the $M_{\star,\rm post}/M_{\star,\rm pre}$ ratio possesses a much stronger correlation to the halo central density. When moving the dividing time by ±0.1 Gyr, the joint Pearson's coefficient decreases by 7 per cent, showing a clear preference for the adopted reionization time across the combined suite. However, differences in the adopted UV background mean that reionization happens at different times between EDGE1 and EDGE2. In EDGE2 taken alone, we see the tightest correlation earlier in time ($t = 0.72$ Gyr; $r = -0.96$). Thus, residual scatter in the EDGE2 results (circles in Fig. 5) is largely accounted for by the fact that we adopt a fixed time for reionization across the combined suite.

3.5 Dependence on the sub-grid model

The extent of baryonic core creation is known to be strongly sensitive to the way in which star formation and feedback are implemented in simulations (Pontzen & Governato 2012; Chan et al. 2015; Oñorbe et al. 2015; Benítez-Llambay et al. 2019). The most important factor for enabling a significant response from the dark matter is that gas reaches densities comparable to the central dark matter cusp, and that a significant fraction of the gas mass repeatedly flows in and out of the central ∼kpc of the galaxy (e.g. Read & Gilmore 2005; Pontzen & Governato 2012, 2014). This naturally occurs if stars form only from high-density gas and there is sufficient numerical resolution to capture the multiphase interstellar medium (Pontzen & Governato 2012; Dutton et al. 2019). Teyssier et al. (2013) highlighted that this results in 'bursty' star formation, with a peak-to-trough ratio of 5–10 and a duty cycle comparable to the local dynamical time. This prediction has been borne out by the data for dwarf galaxy populations (e.g. Kauffmann 2014; McQuinn et al. 2015; Emami et al. 2019, and for a review see Collins & Read 2022).

As mentioned in Section 2, some important changes were introduced in the physics of the new EDGE2 simulations compared to EDGE1. Other than the timing of reionization that we discussed in Section 3.4, the most notable changes relate to the new implementation of non-equilibrium cooling and the inclusion of radiative transfer, which was absent in the majority of EDGE1 runs. These factors result in considerable differences in the galaxy properties, including the SFHs (see Appendix A) and will be discussed more fully in Rey et al. (in preparation).

As a result, EDGE1 haloes end up with higher central densities than EDGE2 haloes. Prior to reionization, the EDGE1 simulations have intense large-scale outflows driven by SNe, which lead to a

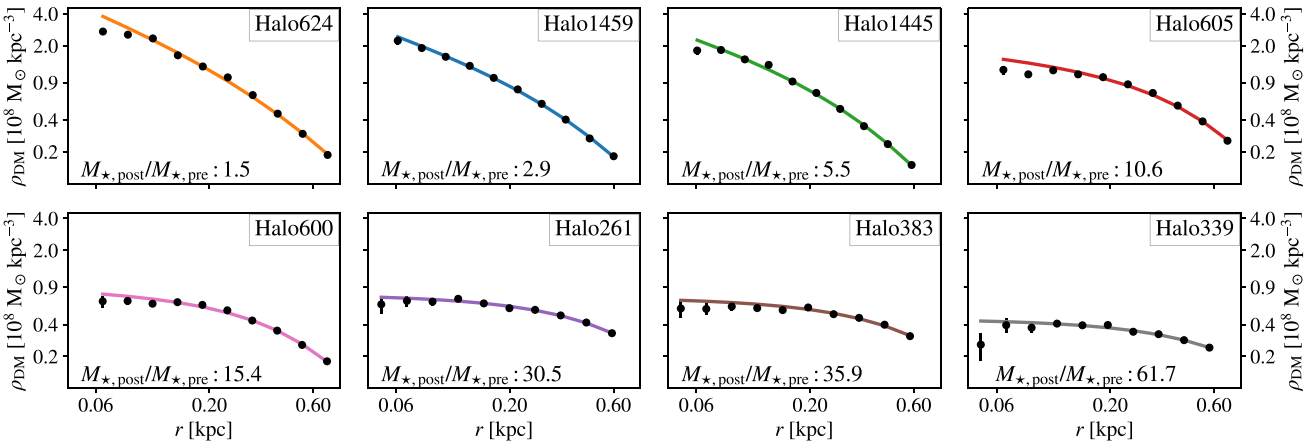

Figure 6. Fit to the density profiles of the EDGE2 haloes using the coreNFW profile. The sizes of the cores are set to be directly proportional to the haloes' half-light radii, and we fit the parameter n, which ranges from an unmodified cusp ($n = 0$) to flat core ($n = 1$). The profiles were cut between $r = 0.05$ and 0.7 kpc to capture the variation in the dark matter central regions across haloes.

hot ($T > 10^6$ K) unbound circumgalactic medium. The radiative feedback adopted in EDGE2 reduces the local intensity of star formation, weakening these outflows and keeping the circumgalactic gas at lower temperatures ($T \sim 10^4$ K) (Agertz et al. 2020), enabling more sustained star formation. As shown in Fig. 2, the different feedback recipes and the changes in the non-equilibrium cooling strength lead to EDGE2 simulations occupying a significantly different locus in the $M_\star/M_{200}$–ρ_{DM} plane compared to EDGE1 simulations.

This difference between suites is almost entirely erased when the central density is seen as a function of $M_{\star,\mathrm{post}}/M_{\star,\mathrm{pre}}$ (Fig. 5), since the new ratio more directly captures the factors determining the central dark matter density. In this picture, EDGE1 and EDGE2 core creation physics appear very similar, but statistically significant differences do remain. When fitting the suites separately to equation (3), the values of the coefficients for EDGE2 with reionization time $t = 0.72$ Gyr are $m_{\mathrm{EDGE2}} = -0.30 \pm 0.04$ and $c_{\mathrm{EDGE2}} = 8.32 \pm 0.06$, and for EDGE1 with reionization time $t = 0.84$ Gyr are $m_{\mathrm{EDGE1}} = -0.24 \pm 0.04$ and $c_{\mathrm{EDGE1}} = 8.08 \pm 0.02$.

In terms of the overall core creation process, these differences are strongly subdominant to the more basic effect that $M_{\star,\mathrm{post}}/M_{\star,\mathrm{pre}}$ changes when moving from EDGE1 to EDGE2 physics. On average, the EDGE1 haloes tend to have lower values of $M_{\star,\mathrm{post}}/M_{\star,\mathrm{pre}}$ than EDGE2, explaining why they also are less prone to forming cores.

As such, the qualitative significance of $M_{\star,\mathrm{post}}/M_{\star,\mathrm{pre}}$ to core formation is preserved regardless of at least some details of the feedback recipe. However, given that EDGE1 and EDGE2 share much of their sub-grid physics in common, it will be of great interest to test whether other simulations with a resolved interstellar medium (e.g. Jeon, Besla & Bromm 2017; Wheeler et al. 2019; Munshi et al. 2021; Gutcke et al. 2022) also predict a major role for $M_{\star,\mathrm{post}}/M_{\star,\mathrm{pre}}$ in core creation.

3.6 Density profiles fitted with coreNFW model

Density profiles in which the central density has been reduced by baryonic feedback can be fitted using a modified version of the classic NFW profile (Navarro, Frenk & White 1997). Read et al. (2016) introduced the coreNFW density profile, which, in addition to the NFW parameters (scale radius r_{s} and density ρ_0), uses two additional variables to describe the core size (r_{c}) and inner density slope (n). The latter ranges from 1 (for a completely flat core) to 0 (for a cuspy NFW profile). See Read et al. (2016), especially their equation (16), for a precise definition. Assuming that the core size is directly proportional to the stellar half-mass radius, De Leo et al. (2024) provided a fit to the remaining parameter n as a function of $M_\star/M_{200}$ based on observational constraints.

To summarize the core creation process seen in our EDGE2 simulation results, we adopt a similar approach. We perform a fit for n (the central density slope) of each dark matter density profile. We also fit the density profiles for M_{200} and c, which control the parameters of the classic NFW profile. We expect the value of n to evolve from $n = 0$ (an NFW cusp) in haloes with small values of $M_{\star,\mathrm{post}}/M_{\star,\mathrm{pre}}$ to $n = 1$ (a flat core) when the feedback-driven outflows become important. There is a degree of degeneracy between n and the core size parameter r_{c}; we break this by setting r_{c} to be directly proportional to the haloes' V-band 3D half-light radii. The constant of proportionality ($\eta = 1.8$) was calculated by letting both n and η vary when fitting the central regions (0.05 kpc $< r <$ 1 kpc) of the profile of Halo339, which has a prominent core, and was then held fixed for all other haloes. Fig. 6 shows the individual fits of the inner regions of the density profiles for the EDGE2 haloes. The density profiles were cut between $r = 0.05$ and 0.7 kpc in order to capture the variation of the profiles' inner regions. The fits are qualitatively good and capture the correct central slopes and core sizes across all the haloes.

Fig. 7 shows the values of n found for each EDGE2 halo as a function of $M_{\star,\mathrm{post}}/M_{\star,\mathrm{pre}}$. The values of n increase with $M_{\star,\mathrm{post}}/M_{\star,\mathrm{pre}}$, capturing the tight relation between our ratio and the amount of 'coreness' in the haloes' inner regions. To parametrize the changes in n, we adopt an analytical function of the form

$$n(x) = \tanh(x/a)^b, \tag{4}$$

where $x = M_{\star,\mathrm{post}}/M_{\star,\mathrm{pre}}$. Fitting to the inferred values of n for the haloes gives $a = 10.27 \pm 1.54$ and $b = 0.86 \pm 0.13$, valid within the range covered by our simulation data ($1 \lesssim M_{\star,\mathrm{post}}/M_{\star,\mathrm{pre}} \lesssim 70$ and $M_\star < 1.5 \times 10^7$ $M_\odot$).

4 CONCLUSION AND DISCUSSION

We presented evidence from the EDGE suite of hydrodynamical simulations that the extent of baryon-driven dark matter core creation strongly depends on the timing of star formation relative to reion-

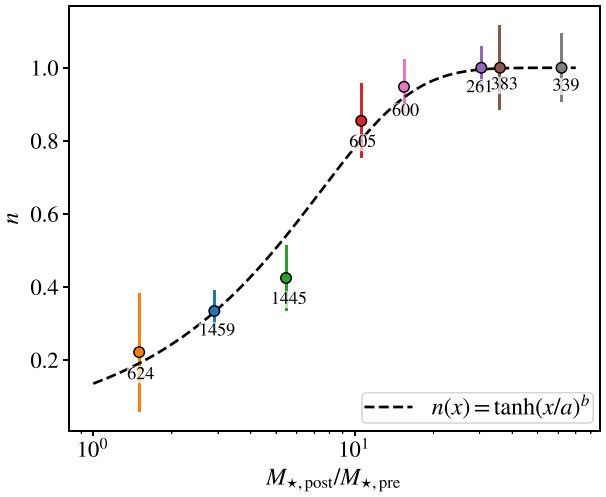

Figure 7. The values of the coreNFW inner slope parameter n found for the EDGE2 haloes as a function of the $M_{\star,\mathrm{post}}/M_{\star,\mathrm{pre}}$ ratios. A value of $n = 0$ means an NFW cusp, while a value of $n = 1$ is a perfect core. The error bars show the 1σ errors on the parameter. The dashed line shows the fitting function given by equation (4).

ization. We focused our study on $\rho_{\mathrm{DM}}(150\,\mathrm{pc})$, the $z = 0$ density of dark matter at 150 pc distance from the halo centre, motivated by the existence of observational estimates in dwarf irregulars and spheroidals at this radius. In the following discussion, we refer to this density as ρ_{DM}, leaving the radius implicit. We find that the EDGE stellar-to-halo mass ratio ($M_\star/M_{200}$) correlates with ρ_{DM} in approximately the way seen in observations. However, we also find that the simulated density correlates much more tightly with a new quantity, $M_{\star,\mathrm{post}}/M_{\star,\mathrm{pre}}$, i.e. the ratio between post- and pre-reionization stellar mass, showing that the timing of star formation is a crucial consideration.

In addition to existing EDGE1 simulations (Agertz et al. 2020; Rey et al. 2020; Orkney et al. 2021), we introduced a new generation of EDGE2 simulations, which extend to higher mass dwarfs and include non-equilibrium cooling. Furthermore, all EDGE2 simulations include photoionization feedback using radiative transfer, whereas the majority of simulations in the EDGE1 suite (including all those presented here) were performed without such a feedback channel. The correlation between ρ_{DM} and $M_{\star,\mathrm{post}}/M_{\star,\mathrm{pre}}$ remains tight when including both suites of simulations, despite radiative transfer and non-equilibrium cooling making a major difference to other observable properties (Agertz et al. 2020). This gives us some confidence that our key conclusions are robust against changes in feedback details. None the less, it will clearly be of considerable interest to investigate our results using alternative state-of-the-art codes (e.g. Jeon et al. 2017; Wheeler et al. 2019; Munshi et al. 2021; Gutcke et al. 2022). All EDGE dwarfs considered are in broad agreement with the SMHM relation inferred from observations, albeit in a mass range where there is considerable uncertainty.

As discussed in Section 1, previous works have focused on $M_\star/M_{200}$ as the primary determinant of core creation. The numerator of this ratio focuses on the total available feedback energy (roughly proportional to $M_\star$). By contrast, the numerator of our revised ratio $M_{\star,\mathrm{post}}$ is a proxy for *sustained* star formation, based on the assumption that dwarfs surviving reionization will continue to form stars over an extended period. Forming stars in a concentrated burst at early times is not an effective way to soften the dark matter cusp (Gnedin & Zhao 2002; Pontzen & Governato 2012; Chan et al. 2015; Jackson et al. 2024); rather, sustained cycles of star formation, gas expulsion, and collapse are required to produce a long-term fluctuating gravitational potential.

M_{200}, which is in the denominator of the traditional ratio, is relevant because it is proportional to the depth of the gravitational potential in which the feedback operates. However, the actual potential to be overcome is not that of the whole halo but rather the concentrated central cusp (i.e. particles do not need to be expelled from the halo as a whole). This central concentration depends on the early accretion history (Ludlow et al. 2014), for which we use $M_{\star,\mathrm{pre}}$ as a proxy that is in principle observable (we discuss observational prospects further below). We also explored the use of other proxies for the central density, such as the maximum circular velocity (v_{max}) (Prada et al. 2012), but found that $M_{\star,\mathrm{post}}/M_{\star,\mathrm{pre}}$ correlates most tightly with ρ_{DM}.

Our stellar masses are calculated across all progenitor branches, and hence $M_{\star,\mathrm{pre}}$ is sensitive to the early collapse of the region as a whole rather than solely of the major progenitor. The correlation with ρ_{DM} becomes less tight when $M_{\star,\mathrm{pre}}$ is evaluated using only the stars formed on the main progenitor branch. A possible reason for this sensitivity to the history of the entire progenitor tree, rather than solely the major progenitor, is that mergers with a steeply cusped halo can increase the central density of the galaxy (Laporte & Penarrubia 2015; Oñorbe et al. 2015; Orkney et al. 2021). We hypothesize that, by incorporating information about all the progenitors in $M_{\star,\mathrm{post}}/M_{\star,\mathrm{pre}}$, this effect is implicitly accounted for.

More broadly, the fact that $M_{\star,\mathrm{post}}/M_{\star,\mathrm{pre}}$ is a good predictor of dark matter density at $z = 0$ reflects the importance of the interplay between reionization and star formation in low-mass galaxies. In future work, we will explore other quantities, which could connect to the halo central density and perform comprehensive studies of the role of formation history by employing genetically modified galaxies (such as late/early formers). We expect $M_{\star,\mathrm{post}}/M_{\star,\mathrm{pre}}$ to play a less essential role in higher mass galaxies, e.g. in determining the cuspiness of MW-mass haloes where stellar feedback is likely ineffective in core creation for different physical reasons (e.g. Di Cintio et al. 2013; Chan et al. 2015; Tollet et al. 2016).

It would be challenging, but very well motivated, to estimate observationally a quantity like $M_{\star,\mathrm{pre}}$. The requirement for $\lesssim$Gyr resolution in an SFH reconstruction over the Hubble time constitutes the major challenge. Even now, however, one can make a qualitative comparison with observed galaxies given recent progress in reconstructing dwarf galaxy SFHs (e.g. Cole et al. 2014; Read et al. 2019; McQuinn et al. 2024). From fig. 5 in Read et al. (2019) and fig. 11 in Bouché et al. (2022), one may indeed infer that galaxies whose star formation stopped a long time ago typically have steeper cusps, while dwarfs with more extended star formation have shallower cores. For instance, Aquarius and LeoII have similar stellar masses and halo masses, but Aquarius has a more extended SFH and a lower central density, as expected if sustained star formation at late times is necessary for the formation of cores.

On the other hand, the observational picture is as yet far from clear-cut; for example, LeoI (Read et al. 2019) seems to have a cuspy profile despite having formed stars until relatively recently. One possibility is that LeoI underwent a recent merger (Ruiz-Lara et al. 2021), enabling it to rebuild a dark matter density cusp (Laporte & Penarrubia 2015; Orkney et al. 2021). This reinforces the need, mentioned above, to explore a greater variety of simulated histories in future work. There has also been speculation about the role that a black hole at the centre of LeoI may have played in its evolution (e.g. Bustamante-Rosell et al. 2021) (although see also Pascale et al. 2024), and we

are in the process of incorporating black holes into the EDGE code for future work.

As discussed in Section 1, the central dark matter densities of low-mass dwarf galaxies hold enormous potential to shed light on particle physics. As such, understanding the confounding effects of baryonic feedback is an essential project, in which the timing of star formation now appears a critical component. To incorporate this rigorously, it will be necessary to interpret forthcoming observations in the light of a broad array of simulations covering a wide variety of formation histories, and making use of codes with a range of alternative feedback prescriptions. However, the tight correlations seen in this work give considerable hope that, in spite of the complexities, baryonic core creation is an essentially predictable process.

ACKNOWLEDGEMENTS

CM would like to thank Dr Jason L. Sanders for the helpful feedback and discussions. CM was supported by the Science and Technology Facilities Council. JIR would like to acknowledge support from STFC grants ST/Y002865/1 and ST/Y002857/1. OA acknowledges support from the Knut and Alice Wallenberg Foundation, the Swedish Research Council (grant 2019-04659), and the Swedish National Space Agency (SNSA Dnr 2023-00164). MPR was supported by the Beecroft Fellowship funded by Adrian Beecroft. ET acknowledges the UKRI Science and Technology Facilities Council (STFC) for support (grant ST/V50712X/1). This study was supported by the European Research Council (ERC) under the European Union's Horizon 2020 research and innovation programme (grant agreement no. 818085 GMGalaxies). This work was performed in part using the DiRAC Data Intensive service at Leicester, operated by the University of Leicester IT Services, which forms part of the STFC DiRAC HPC Facility (www.dirac.ac.uk). The equipment was funded by BEIS capital funding via STFC capital grants ST/K000373/1 and ST/R002363/1 and STFC DiRAC Operations grant ST/R001014/1. DiRAC is part of the National e-Infrastructure. This work was partially enabled by funding from the UCL Cosmoparticle Initiative.

The contributions from the authors are listed below using key words based on the CRediT (Contribution Roles Taxonomy) system. **CM:** conceptualization; investigation; methodology; software; formal analysis; visualization; writing – original draft, review, and editing. **AP:** conceptualization; methodology; validation and interpretation; supervision; resources; writing – original draft, review, and editing; funding acquisition. **JIR:** conceptualization; methodology; validation and interpretation; writing – review and editing. **OA:** methodology; writing – review and editing. **MPR:** software, data curation, and resources. **ET:** writing – review and editing. **SYK:** writing – review and editing. **EIG:** data curation; writing – review and editing.

DATA AVAILABILITY

Data may be shared upon reasonable request.

REFERENCES

Adams J. J. et al., 2014, ApJ, 789, 63
Agertz O. et al., 2020, MNRAS, 491, 1656
Aubert D., Pichon C., Colombi S., 2004, MNRAS, 352, 376
Behroozi P. S., Conroy C., Wechsler R. H., 2010, ApJ, 717, 379
Benítez-Llambay A., Frenk C. S., Ludlow A. D., Navarro J. F., 2019, MNRAS, 488, 2387
Benson A. J., Lacey C. G., Baugh C. M., Cole S., Frenk C. S., 2002, MNRAS, 333, 156
Binney J., Mamon G. A., 1982, MNRAS, 200, 361
Bouché N. F. et al., 2022, A&A, 658, A76
Bullock J. S., Boylan-Kolchin M., 2017, ARA&A, 55, 343
Bustamante-Rosell M. J., Noyola E., Gebhardt K., Fabricius M. H., Mazzalay X., Thomas J., Zeimann G., 2021, ApJ, 921, 107
Chan T. K., Kereš D., Oñorbe J., Hopkins P. F., Muratov A. L., Faucher-Giguère C.-A., Quataert E., 2015, MNRAS, 454, 2981
Christensen C. R., Brooks A. M., Munshi F., Riggs C., Van Nest J., Akins H., Quinn T. R., Chamberland L., 2024, ApJ, 961, 236
Cole A. A., Weisz D. R., Dolphin A. E., Skillman E. D., McConnachie A. W., Brooks A. M., Leaman R., 2014, ApJ, 795, 54
Collins M. L. M., Read J. I., 2022, Nat. Astron., 6, 647
Cooke L. H. et al., 2022, MNRAS, 512, 1012
Courty S., Alimi J. M., 2004, A&A, 416, 875
Danieli S., Greene J. E., Carlsten S., Jiang F., Beaton R., Goulding A. D., 2023, ApJ, 956, 6
De Leo M., Read J. I., Noel N. E. D., Erkal D., Massana P., Carrera R., 2024, MNRAS, 535, 1015
Dekel A., Silk J., 1986, ApJ, 303, 39
Di Cintio A., Brook C. B., Macciò A. V., Stinson G. S., Knebe A., Dutton A. A., Wadsley J., 2013, MNRAS, 437, 415
Di Cintio A., Brook C. B., Macciò A. V., Stinson G. S., Knebe A., Dutton A. A., Wadsley J., 2014, MNRAS, 437, 415
Dutton A. A., Macciò A. V., Buck T., Dixon K. L., Blank M., Obreja A., 2019, MNRAS, 486, 655
Efstathiou G., 1992, MNRAS, 256, 43P
Efstathiou G., 2000, MNRAS, 317, 697
Eisenstein D. J., Hut P., 1998, ApJ, 498, 137
El-Zant A., Shlosman I., Hoffman Y., 2001, ApJ, 560, 636
Emami N., Siana B., Weisz D. R., Johnson B. D., Ma X., El-Badry K., 2019, ApJ, 881, 71
Fattahi A., Navarro J. F., Frenk C. S., Oman K. A., Sawala T., Schaller M., 2018, MNRAS, 476, 3816
Faucher-Giguère C.-A., 2020, MNRAS, 493, 1614
Garrison-Kimmel S., Bullock J. S., Boylan-Kolchin M., Bardwell E., 2017, MNRAS, 464, 3108
Gnedin O. Y., Zhao H., 2002, MNRAS, 333, 299
Governato F. et al., 2010, Nature, 463, 203
Gray E. I. et al., 2024, preprint (arXiv:2405.19286)
Gutcke T. A., Pakmor R., Naab T., Springel V., 2022, MNRAS, 513, 1372
Haardt F., Madau P., 1996, ApJ, 461, 20
Hu W., Barkana R., Gruzinov A., 2000, Phys. Rev. Lett., 85, 1158
Jackson R. A. et al., 2024, MNRAS, 528, 1655
Jeon M., Besla G., Bromm V., 2017, ApJ, 848, 85
Kauffmann G., 2014, MNRAS, 441, 2717
Kim S. Y. et al., 2024, preprint (arXiv:2408.15214)
Laporte C. F. P., Penarrubia J., 2015, MNRAS, 449, L90
Ludlow A. D., Navarro J. F., Angulo R. E., Boylan-Kolchin M., Springel V., Frenk C., White S. D. M., 2014, MNRAS, 441, 378
McQuinn K. B. W., Lelli F., Skillman E. D., Dolphin A. E., McGaugh S. S., Williams B. F., 2015, MNRAS, 450, 3886
McQuinn K. B. W., Mao Y.-Y., Tollerud E. J., Cohen R. E., Shih D., Buckley M. R., Dolphin A. E., 2024, ApJ, 967, 161
Marasco A., Oman K. A., Navarro J. F., Frenk C. S., Oosterloo T., 2018, MNRAS, 476, 2168
Mashchenko S., Wadsley J., Couchman H. M. P., 2008, Science, 319, 174
Mina M., Mota D. F., Winther H. A., 2022, A&A, 662, A29
Moster B. P., Naab T., White S. D. M., 2013, MNRAS, 428, 3121
Muni C., Pontzen A., Sanders J. L., Rey M. P., Read J. I., Agertz O., 2023, MNRAS, 527, 9250
Munshi F., Brooks A. M., Applebaum E., Christensen C. R., Quinn T., Sligh S., 2021, ApJ, 923, 35
Mutlu-Pakdil B. et al., 2019, ApJ, 885, 53
Nadler E. O. et al., 2020, ApJ, 893, 48
Navarro J. F., Eke V. R., Frenk C. S., 1996, MNRAS, 283, L72
Navarro J. F., Frenk C. S., White S. D. M., 1997, ApJ, 490, 493

Newton O. et al., 2021, J. Cosmol. Astropart. Phys., 2021, 062
Nipoti C., Binney J., 2014, MNRAS, 446, 1820
Oman K. A. et al., 2015, MNRAS, 452, 3650
Oman K. A., Marasco A., Navarro J. F., Frenk C. S., Schaye J., Benítez-Llambay A., 2018, MNRAS, 482, 821
Oñorbe J., Boylan-Kolchin M., Bullock J. S., Hopkins P. F., Kereš D., Faucher-Giguère C.-A., Quataert E., Murray N., 2015, MNRAS, 454, 2092
Orkney M. D. A. et al., 2021, MNRAS, 504, 3509
Pace A. B., Erkal D., Li T. S., 2022, ApJ, 940, 136
Pascale R., Nipoti C., Calura F., Della Croce A., 2024, A&A, 684, L19
Peñarrubia J., Pontzen A., Walker M. G., Koposov S. E., 2012, ApJ, 759, L42
Planck Collaboration XVI, 2014, A&A, 571, A16
Pontzen A., Governato F., 2012, MNRAS, 421, 3464
Pontzen A., Governato F., 2014, Nature, 506, 171
Pontzen A., Tremmel M., 2018, ApJS, 237, 23
Pontzen A., Roškar R., Stinson G., Woods R., 2013, Astrophysics Source Code Library, record ascl:1305.002
Power C., Navarro J. F., Jenkins A., Frenk C. S., White S. D. M., Springel V., Stadel J., Quinn T., 2003, MNRAS, 338, 14
Prada F., Klypin A. A., Cuesta A. J., Betancort-Rijo J. E., Primack J., 2012, MNRAS, 423, 3018
Read J. I., Gilmore G., 2005, MNRAS, 356, 107
Read J. I., Agertz O., Collins M. L. M., 2016, MNRAS, 459, 2573
Read J. I., Iorio G., Agertz O., Fraternali F., 2017, MNRAS, 467, 2019
Read J. I., Walker M. G., Steger P., 2019, MNRAS, 484, 1401
Rey M. P., Pontzen A., Agertz O., Orkney M. D. A., Read J. I., Saintonge A., Pedersen C., 2019, ApJ, 886, L3
Rey M. P., Pontzen A., Agertz O., Orkney M. D. A., Read J. I., Rosdahl J., 2020, MNRAS, 497, 1508
Rey M. P., Pontzen A., Agertz O., Orkney M. D. A., Read J. I., Saintonge A., Kim S. Y., Das P., 2022, MNRAS, 511, 5672
Rocha M., Peter A. H. G., Bullock J. S., Kaplinghat M., Garrison-Kimmel S., Oñorbe J., Moustakas L. A., 2013, MNRAS, 430, 81
Roper F. A., Oman K. A., Frenk C. S., Benítez-Llambay A., Navarro J. F., Santos-Santos I. M. E., 2023, MNRAS, 521, 1316
Rosdahl J., Blaizot J., Aubert D., Stranex T., Teyssier R., 2013, MNRAS, 436, 2188
Ruiz-Lara T. et al., 2021, MNRAS, 501, 3962
Schive H.-Y., Liao M.-H., Woo T.-P., Wong S.-K., Chiueh T., Broadhurst T., Hwang W.-Y. P., 2014, Phys. Rev. Lett., 113, 261302
Schneider A., Smith R. E., Macciò A. V., Moore B., 2012, MNRAS, 424, 684
Shipp N. et al., 2018, ApJ, 862, 114
Simon J. D., 2019, ARA&A, 57, 375
Stopyra S., Pontzen A., Peiris H., Roth N., Rey M. P., 2021, ApJS, 252, 28
Teyssier R., 2002, A&A, 385, 337
Teyssier R., Pontzen A., Dubois Y., Read J. I., 2013, MNRAS, 429, 3068
Tollet E. et al., 2016, MNRAS, 456, 3542
Tulin S., Yu H.-B., 2018, Phys. Rep., 730, 1
Tweed D., Devriendt J., Blaizot J., Colombi S., Slyz A., 2009, A&A, 506, 647
Weerasooriya S., Bovill M. S., Benson A., Musick A. M., Ricotti M., 2023, ApJ, 948, 87
Wheeler C. et al., 2019, MNRAS, 490, 4447
Yoshida N., Springel V., White S. D. M., Tormen G., 2000, ApJ, 544, L87
Zoutendijk S., Brinchmann J., Bouché N., den Brok M., Krajnovic D., Kuijken K., Maseda M., Schaye J., 2021, A&A, 651, A80

APPENDIX A: CONTRASTING EDGE1 AND EDGE2 STAR FORMATION HISTORIES

As discussed in Section 2, several changes in the sub-grid physics have been introduced between the EDGE1 suite and the new EDGE2 iterations. Here, we look at the response that changing the feedback recipe has on the SFHs.

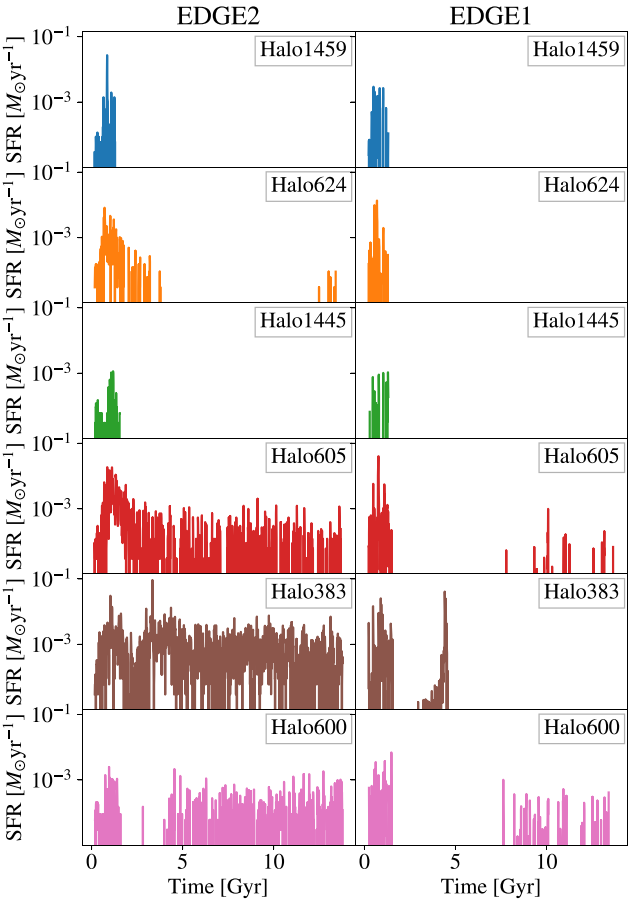

Figure A1. Comparison between the SFHs of haloes in EDGE1 and in EDGE2. The addition of radiative transfer in EDGE2 weakens early large-scale outflows and keeps the gas at lower temperatures, allowing more extended star formation until $z = 0$.

Six of the eight haloes implemented in EDGE2 have equivalents in the EDGE1 runs. Fig. A1 shows a direct comparison between the SFHs of the haloes in the two simulation suites. The EDGE1 runs see intense large-scale outflows at high redshift, which are driven by SNe, leading to a very hot circumgalactic medium. The addition of radiative transfer in EDGE2 weakens these outflows and keeps the gas at lower temperatures, which, especially combined with the addition of non-equilibrium cooling physics, allows more stars to form. These changes have a clear effect on the SFH, particularly sustaining star formation at late times. Although this is less obvious in the cuspier haloes (1459, 624, and 1445), the ones with the strongest cores in EDGE2 (383, 600, and 605) have much greater post-reionization star formation activity than in their EDGE1 counterparts. As discussed in the main text, this difference leads directly to EDGE1 haloes remaining cuspier than their EDGE2 counterparts, in a way that cannot be captured by $M_\star/M_{200}$.

This paper has been typeset from a TEX/LATEX file prepared by the author.